Published in final edited form as:
J Immunol. 2013 April 1; 190(7): 3570–3578. doi:10.4049/jimmunol.1202076.

Functional macrophage heterogeneity in a mouse model of autoimmune CNS pathology

Anat London[2,*], **Inbal Benhar**[2,*], **Mary J. Mattapallil**[†], **Matthias Mack**[‡], **Rachel R. Caspi**[†], and **Michal Schwartz**[3,*]

[*]Department of Neurobiology, Weizmann Institute of Science, Rehovot, Israel

[†]Laboratory of Immunology, National Eye Institute/NIH, Bethesda, MD

[‡]Department of Internal Medicine, University of Regensburg, Regensburg, Germany

Abstract

Functional macrophage heterogeneity is well appreciated outside the CNS in wound healing and cancer, and was recently also demonstrated in several CNS compartments following “sterile” insults. Yet, such heterogeneity was largely overlooked in the context of inflammatory autoimmune pathology, in which macrophages were mainly associated with disease induction and propagation. Here, we show the diversity of monocyte-derived macrophages along the course of experimental autoimmune uveitis (EAU), an inflammatory condition affecting the ocular system, serving a model for CNS autoimmune pathology. Disease induction resulted in the appearance of a distinct myeloid population in the retina, and in the infiltration of monocyte-derived macrophages that were absent from control eyes. During the disease course, the frequency of CX_3CR1^{high} infiltrating macrophages that express markers associated with inflammation-resolving activity was increased, along with a decrease in the frequency of inflammation-associated, $Ly6C^+$ macrophages. Inhibition of monocyte infiltration at the induction phase of EAU prevented disease onset, while monocyte depletion at the resolution phase resulted in a decrease in $Foxp3^+$ regulatory T cells, and in exacerbated disease. Thus, monocyte-derived macrophages display distinct phenotypes throughout the disease course, even in an immune-induced pathology, reflecting their differential roles in disease induction and resolution.

[3]Address correspondence and reprint requests to Prof. Michal Schwartz, Weizmann Institute of Science, Department of Neurobiology, Rehovot, 76100, Israel, Tel, 972-8-9342467, Fax, 972-8-9346018, Cell, 972-54-5660497, michal.schwartz@weizmann.ac.il, http://www.weizmann.ac.il/neurobiology/labs/schwartz/.

[2]A.L. and I.B. contributed equally to this work.

[1]This work was supported in part by the Glaucoma Research Foundation and the European Research Council Advanced Grant (Agreement Number: 232835). R.R.C. was funded by NIH/NEI intramural funding, Project #EY000184-29.

Author Contributions

A.L. and I.B. designed and performed the research, collected, analyzed and interpreted the data, performed statistical analysis and wrote the manuscript.
M.J.M analyzed the rd8 status of the mice.
M.M. contributed the MC-21 antibody.
R.R.C. participated in designing the research and establishing the EAU model, and contributed to writing the manuscript.
M.S. designed the research, interpreted the data and wrote the manuscript.

Conflict of Interest Disclosures

The authors have no conflicting financial interests.

[4]Abbreviations used in this article: BM, bone marrow; EAU, experimental autoimmune uveitis; IRBP, interphotoreceptor retinoid-binding protein; Treg, regulatory T cell; WT, wild type.

Introduction

Macrophages are key players in settings of sterile insults as well as under infectious conditions and in cancer. Outside the CNS, the heterogeneity and multi-functionality of these cells is well-substantiated (1-4). Monocyte-derived macrophages, which infiltrate the tissue upon insult, have generally been divided into two subsets; $CCR2^{+}CX_3CR1^{low}Ly6C^{+}$ monocyte-derived macrophages are the first recruited in response to insult and exhibit a typical pro-inflammatory phenotype, while the second subset, comprised of $CCR2^{-}CX_3CR1^{high}Ly6C^{-}$ cells, takes part in immune resolution (2, 5-7). Macrophages are also broadly divided, based on their activation state, into two polarized phenotypes known as M1, or classically-activated macrophages, and M2, or alternatively-activated macrophages (3), which include “resolution-phase macrophages” (8). Recently, Mosser and Edwards suggested classifying macrophages based on their functions in helping to maintain homeostasis, namely: host defense, wound healing and immune regulation (4). All of these classifications indicate the diversity of macrophage populations, displaying functions that reflect the changing needs of the tissue along the course of healing (5, 7), including clearance of dead cells and cellular debris, as well as secretion of pro- and anti-inflammatory molecules and growth factors. The timing and duration of the macrophage response, as well as their phenotype, which depends on the local milieu within the tissue and on their route of trafficking (4, 9), all together determine the fate of the tissue.

In the CNS, macrophage heterogeneity has been demonstrated under various sterile inflammatory conditions and in models of neurodegenerative disease (10-13). Those studies functionally distinguished between resident microglia, the native myeloid cells of the CNS, and blood-borne monocyte-derived macrophages that infiltrate the CNS only following an insult. Monocyte-derived macrophages have been shown to serve as resolution-phase macrophages, required to bring about the proper termination of the immune response and the restoration of homeostasis in the tissue, thereby promoting neuroprotection and neurorepair (10, 11, 14). In this study, we explored the possibility that distinct subsets of macrophages are differentially involved in coping with autoimmune CNS pathology, using the model of experimental autoimmune uveitis (EAU). EAU is induced in mice by immunization with retinal antigens, and is a model for human posterior uveitis, a potentially blinding inflammatory ocular condition that affects the choroid of the eye and the neural retina (15, 16). Many studies have identified macrophages as key players in EAU, mainly in the context of the induction and effector phase of the disease (17, 18), although several reports have indicated the presence of macrophages in the resolution stage, as well (19, 20). However, in most of these studies there was no functional distinction between resident microglia and infiltrating macrophages. In addition, the current state of knowledge on macrophage involvement in EAU reinforces the need for characterizing distinct subsets of monocyte-derived macrophages and their functions at different phases of the disease *in vivo*.

Here, we followed the changes in myeloid populations along the course of EAU, and identified infiltration of monocyte-derived macrophages into diseased retinas. We found that these cells are comprised of CX_3CR1^{high} and CX_3CR1^{low} macrophage populations, whose kinetics change along the disease course. The frequency of CX_3CR1^{high} macrophages was highest at the peak of disease, and remained elevated throughout the resolution phase; these cells were found to express higher levels of resolution-associated surface markers compared to their CX_3CR1^{low} counterparts. Inhibition of monocyte-derived macrophage infiltration at disease onset prevented EAU, whereas inhibition of this infiltration after the peak of disease resulted in a decrease in $Foxp3^{+}$ regulatory T cells in the retina, and in worse disease outcome. These results indicate that monocyte-derived macrophages are functionally heterogeneous in a CNS autoimmune disease, and may differentially contribute to disease resolution as compared to disease induction. Thus, particular macrophage subsets can play a

role in disease resolution, even in a pathology that is primarily induced by an aberrant immune response.

Methods

Mice

Adult male (8–10 wk old) C57BL/6J mice and heterozygous *Cx3cr1*$^{GFP/+}$ transgenic mice (B6.129P-*Cx3cr1*^{tm1Litt}/J, in which one of the CX_3CR1 chemokine receptor alleles is replaced with a gene encoding GFP (21)) were used. These mice were tested and found negative for the rd8 mutation (22). *Foxp3*^{GFP} mice were a generous gift from Dr. Alexander Rudensky. Animals were supplied by the Animal Breeding Center of the Weizmann Institute of Science. All experiments conformed to the regulations formulated by the Institutional Animal Care and Use Committee of the Weizmann Institute of Science.

Preparation of bone marrow (BM) chimeras

To create [*Cx3cr1*$^{GFP/+}$ → WT] BM chimeric mice, WT recipient mice received lethal whole-body irradiation (950 rad) while shielding the head, as previously described (11, 23). This shielding prevented any direct effects on the retina and/or infiltration of myeloid cells other than those related to disease induction. On the next day, mice were reconstituted with 5×10^6 *Cx3cr1*$^{GFP/+}$ BM cells according to a previously described protocol (11). This protocol results in BM chimerism rates of 50%-70%. Chimeric mice were subjected to EAU induction 8–12 wk after BM transplantation.

EAU induction and scoring

Native bovine interphotoreceptor retinoid-binding protein (IRBP) was produced as described previously (24). The uveitogenic 20 amino acid peptide representing residues 1–20 of IRBP ($IRBP_{1\text{-}20}$) (25) was synthesized by AnaSpec, Fremont CA, by GL Biochem Ltd., Shanghai, or by the peptide synthesis unit at the Weizmann Institute. Mice were immunized subcutaneously with 500 μg peptide or with 300 μg peptide plus 150 μg native bovine IRBP as a 1:1 emulsion with CFA containing *Mycobacterium tuberculosis* strain H37.RA at 2.5 mg/ml (1.25 mg/ml final). Mice were co-injected with 1 μg Bordella pertussis toxin (Sigma) intraperitoneally. In this model, which induced disease in 80-100% of the mice, clinical onset is described around d15, and disease peak is between d22-d29 (26-28).

For EAU scoring, eyes were processed for histopathology on day 35 after immunization, and stained with hematoxylin and eosin. EAU severity was evaluated in a blinded fashion on a scale of 0–4, using previously published criteria (29, 30).

MC-21 administration

MC-21, an antibody to CCR2 (31), which selectively depletes $Ly6C^+$ monocytes from the peripheral blood, was injected intraperitoneally before or after the peak of EAU, every other day for a total of 5 injections (8 μg per injection).

Immunohistochemistry

After intracardiac perfusion with PBS, eyes were removed, fixed in 2.5% paraformaldehyde (PFA) for 24 h, transferred to 70% ethanol and then embedded in paraffin, as previously described (32). For clinical scoring, eyes were immersed for 1 h in 4% phosphate-buffered glutaraldehyde and transferred into 10% phosphate-buffered formaldehyde until processing. Representative sections were stained with hematoxylin and eosin for histopathological examination. The following antibodies were used for immunolabeling: rabbit anti-GFP (1:100; MBL), mouse anti-Brn3a (1:50; Santa Cruz Biotechnology, Inc.), goat anti-IL-10

(1:20; R&D Systems). The M.O.M. immunodetection kit (Vector Laboratories) was used to localize mouse primary monoclonal antibodies. For activated myeloid cell labeling, FITC-conjugated Bandeiraea simplicifolia isolectin B4 (IB-4; 1:50; Sigma-Aldrich) was added for 1 h to the secondary antibody solution. Secondary antibodies used included Cy2/Cy3-conjugated donkey anti–mouse, –rabbit, or –goat antibodies (1:150-1:200, all from Jackson ImmunoResearch Laboratories, Inc.). The slides were exposed to Hoechst stain (1:2,000; Invitrogen) for 1 min. For microscopic analysis, a fluorescence microscope (Eclipse 80i; Nikon) was used. The fluorescence microscope was equipped with a digital camera (DXM1200F; Nikon) and with either a 20× NA 0.50 or 40× NA 0.75 objective lens (Plan Fluor; Nikon). Recordings were made on postfixed tissues at 24°C using NIS-Elements, F3 (Nikon) acquisition software. Images were cropped, merged, and optimized using Photoshop (Adobe), by making minor adjustments to contrast, and were arranged using Canvas X (Deneba Software).

Isolation of retinal cells and flow cytometry

Following intracardiac perfusion with PBS, retinas were removed by dissection and processed to single-cell suspension, as previously described (19, 33). The following fluorochrome-labeled mAbs were purchased from BD, BioLegend, eBioscience or AbD Serotec, and used according to the manufacturers' protocols: PE-conjugated anti-CD11b, CD206 (MMR), and IL-4Rα antibodies; PerCP-cy5.5-conjugated anti-Ly6C and CD11b antibodies; allophycocyanin (APC)-conjugated anti-CD115, TCRβ, Foxp3 and CD204 antibodies, Alexa 647-conjugated anti-Dectin-1 antibody; and Pacific Blue/Brilliant Violet-conjugated anti-TCRβ, CD4 and CD45.2 antibodies. Foxp3 staining was performed using the Foxp3 staining buffer set (eBioscience), and IL-10 staining was performed using Mouse IL-10 Secretion Assay Detection Kit (Miltenyi Biotec), according to manufacturers' protocols. Cells were analyzed on a FACS LSRII cytometer using FACSDiva software (both from BD). Analysis was performed with FlowJo software (Tree Star, Inc.). In each experiment, relevant negative and positive control groups were used to determine the populations of interest and to exclude the rest.

Statistical Analysis

Levene's test was used to check equality of variance. In the case of equal variances, data were analyzed using a Student's t test to compare between two groups, or by one-way ANOVA to compare several groups. Tukey's HSD test was used for follow-up pairwise comparison of groups after the null hypothesis was rejected ($p < 0.05$). In the case of unequal variances, data were log-transformed to achieve equal variances when possible; otherwise, the Kruskal-Wallis test was used to compare several groups, followed by Dunn's test. EAU scores were analyzed by Mann Whitney's U test. Results are presented as mean ± SE, and y-axis error bars in the graphs represent SE unless indicated otherwise.

Results

Changes in myeloid populations after EAU induction

EAU was induced in mice by immunization with a uveitogenic regimen of $IRBP_{1-20}$, as described in Methods. This regimen induced disease in 80–100% of animals by 14 days after immunization. To track changes in mononuclear myeloid cells following induction of EAU, we first used mice that express GFP under the CX_3CR1 promoter (21). In these mice, the GFP label enables the entire mononuclear myeloid population to be followed, with no distinction between resident microglia and infiltrating monocyte-derived macrophages. Mice were left untreated (naïve), or immunized with either IRBP/CFA or PBS/CFA. Immunohistochemical staining for GFP at time points corresponding to the peak of disease, which occurs between d22 and d29 after immunization (25, 27, 28, 34), revealed numerous

$CX_3CR1\text{-}GFP^+$ myeloid cells dispersed among the retinal layers in the IRBP/CFA group. Some of these cells were localized to the photoreceptor layer and the ganglion cell layer (GCL; Fig. 1 a). Co-staining with the retinal ganglion cell (RGC) marker, Brn3a, revealed a distorted GCL, which likely reflects damage to the RGCs as part of EAU pathology (Fig. 1 a). The myeloid cells were found to be distributed in the vitreous and among the retinal layers, and stained positive for the myeloid activation marker, IB-4 (Fig. 1 b). Flow cytometric analysis of retinas on d22 after immunization showed a general increase in the number of leukocytes, detected by CD45 staining, in diseased retinas as compared to controls (naïve, PBS/CFA) (Fig. 1 c left panels, d). In addition, we observed a significant increase in the numbers of $CD11b^+CX_3CR1\text{-}GFP^+$ myeloid cells in diseased retinas (Fig. 1 c middle panels, e). Specifically, we detected a change in myeloid populations in the IRBP/CFA-injected mice; whereas retinas from naïve mice, as well as from PBS/CFA controls included a sparse population of $CD11b^+CX_3CR1\text{-}GFP^{high}$ myeloid cells (Fig. 1 c i, ii), IRBP/CFA retinas showed, in addition to an increase in this population, a second, distinct, $CD11b^+CX_3CR1\text{-}GFP^{low}$ subset (Fig. 1 c iii). Thus, EAU induced changes in the myeloid populations within the retina. These changes might reflect expansion and phenotype change of the resident myeloid cells, and/or the infiltration of an additional population from the blood.

Monocyte-derived macrophages infiltrate uveitic retinas

To address the question of whether the changes detected in myeloid populations include recruitment of monocytes from the blood, we performed the EAU immunization protocol on [$Cx_3cr1^{GFP/+}$ ➔ WT] bone marrow (BM) chimeric mice, whose WT BM was replaced with that of $Cx_3cr1^{GFP/+}$ mice, and followed the infiltration of monocyte-derived macrophages into the retina at several time points after EAU induction. In these chimeras, it is possible to distinguish between infiltrating monocyte-derived macrophages and resident microglia, as only the infiltrating cells, derived from donor BM, are labeled with GFP.

Retinas from chimeric mice that received PBS/CFA showed no infiltration of circulating monocytes at any time point after immunization, as seen by both flow cytometric and immunohistochemical analyses, and were identical to naïve mice, (Fig. 2 a, b and c, **top panel**). On the other hand, retinas of IRBP/CFA mice contained many infiltrating GFP^+ monocyte-derived macrophages (Fig. 2 a-c), which were scattered among the retinal layers and were found in a state of activation, as seen by IB-4 staining (Fig. 2 c, **bottom panel**). We followed the kinetics of this infiltration along the disease course and found that the time of peak monocyte infiltration corresponded to the peak of disease in this model, namely d22-d29 post immunization (Fig. 2 d). Of note, the $CD11b^+CX_3CR1\text{-}GFP^{neg}$ population, mostly representing the resident myeloid cells (and possibly neutrophils, to some extent), was also found to increase along the course of EAU (from 237.21±127.96 cells at EAU onset (d15) to 782.61±235.73 at disease peak (d22), $p<0.001$).

Interestingly, some of the infiltrating macrophages were found to express the anti-inflammatory cytokine, IL-10, as was demonstrated both by flow cytometry and immunohistochemical staining starting from the peak of EAU (Fig. 2. e, f). As the immune infiltrate in uveitis is usually considered a measure of inflammation and disease severity, detecting the expression of this classical anti-inflammatory cytokine by some of the infiltrating macrophages suggests that the macrophage infiltrate in this disease is rather heterogeneous.

Monocyte-derived macrophage heterogeneity over the course of EAU

In order to address macrophage heterogeneity in EAU, we induced the disease in [$Cx_3cr1^{GFP/+}$ ➔ WT] BM chimeric mice and evaluated the phenotype of the infiltrating

macrophages in the retina using flow cytometry. Several studies that characterized subgroups of monocyte-derived macrophages in insults outside the CNS, divided these cells into two main subsets based on the expression of two markers: the $CX_3CR1^{low}Ly6C^+$ and $CX_3CR1^{high}Ly6C^-$ populations, corresponding to pro- and anti-inflammatory phenotypes, respectively (5, 7). Gating on the infiltrating monocyte-derived macrophages at the peak of EAU, we found that these cells could be subdivided based on the intensity of CX_3CR1-GFP expression (Fig. 3 a). The frequency of CX_3CR1-GFP^{high} macrophages was low at the onset of disease, after which it began to increase, reaching peak levels at d22, the peak of disease, which, in effect, marks the beginning of resolution; this population remained high throughout the resolution phase (Fig. 3 b). In line with this increase, the frequency of $Ly6C^+$ macrophages, corresponding to the pro-inflammatory subset, was highest at disease onset and decreased by d22, remaining relatively low at the later stages of EAU (Fig. 3 c). We found that the initial appearance of the CX_3CR1-GFP^{high} macrophages corresponded to the timing of the beginning of the resolution phase. This observation, together with the well-recognized contribution of the CX_3CR1^{high} population to wound healing and repair under injurious conditions in non-CNS tissues, prompted us to examine the possibility that this subset might also take part in the resolution of EAU. We therefore tested these cells for expression of markers known to be associated with immune resolution and wound healing, namely CD206 (mannose receptor), Dectin-1, CD204 (macrophage scavenger receptor 1) and IL-4Rα (8, 35-38). At all time points tested, these markers were found to be expressed at higher levels among the CX_3CR1-GFP^{high} population, as compared to the CX_3CR1-GFP^{low} cells (Fig. 3 d). Notably, the CX_3CR1-GFP^{high} population was found to express lower levels of Ly6C relative to its CX_3CR1-GFP^{low} counterpart, reminiscent of the anti-inflammatory monocyte subset described by others (5, 7).

In CNS insult, another level of complexity is introduced when taking into account the microglia, the resident immune population of the CNS, which have a low rate of turnover by cell renewal, independently of circulating monocytes (39-41), and actively participate in the local inflammatory response. In order to gain insight regarding the phenotype of the resident myeloid cells, we gated on the CX_3CR1-GFP^{neg} population in retinas from [$Cx_3cr1^{GFP/+}$ → WT] BM chimeric mice. Interestingly, the frequencies at which the resolution markers were expressed within this population were significantly low compared to the CX_3CR1-GFP^{high} infiltrating macrophages, and comparable to those of the CX_3CR1-GFP^{low} macrophages. However, the resident cells expressed Ly6C at a lower frequency than the CX_3CR1-GFP^{low} macrophages (Fig. 3 d).

Together, these results demonstrate the diverse phenotypes displayed by macrophages in EAU, and suggest that this heterogeneity may also be reflected in terms of their function, which may affect disease outcome.

Early recruitment of monocyte-derived macrophages is required to induce EAU

In view of the significant phenotypic differences we found between the two subsets of infiltrating monocyte-derived macrophages, we next turned to explore the roles of these cells at different phases of EAU. Because the CX_3CR1-GFP^{high} macrophages, which exhibited a resolving phenotype, appeared at the beginning of the resolution phase, we hypothesized that inhibiting macrophage infiltration before the peak of EAU as compared to after the peak, would result in different disease outcomes.

By making use of the anti-CCR2 antibody, MC-21, which depletes $Ly6C^+$ monocytes from the blood (31), we were able to greatly reduce their infiltration into the retinas of IRBP/CFA-immunized mice (Fig. 4 a-c). Such depletion starting before the onset of EAU resulted in diminished T cell infiltration into the retina as analyzed at d22 after immunization, so that these retinas retained an appearance comparable to those of PBS/CFA-immunized (control)

mice (Fig. 4 d, e). Histological examination revealed that, as opposed to retinas from untreated IRBP/CFA-immunized mice that developed full-blown disease, retinas from MC-21-treated mice did not display the typical histopathological features of EAU, namely vasculitis, retinal folding, and distortion of the retinal layers (29) (Fig. 4 f). These results indicated that monocyte-derived macrophages recruited early in the disease process are involved in the induction of EAU pathology.

Monocyte-derived macrophages at the later phase of EAU contribute to disease resolution

In order to determine whether monocyte-derived macrophages are also involved in the resolution phase of EAU, we used the MC-21 antibody for the depletion of monocyte-derived macrophages starting at the peak of disease (Fig. 5 a), a time when the CX_3CR1-GFP^{high} population, reminiscent of resolution-phase macrophages, was at its highest (Fig. 3 b). This depletion regimen resulted in lower numbers of CX_3CR1-GFP^+ infiltrating macrophages in the retina (Fig. 5 b). Levels of $Foxp3^+$ regulatory T cells (Tregs), whose elevation is characteristic of an inflammation-resolving milieu, and which have been associated with resolution of EAU (19, 42-45, and Silver PB et al., manuscript in preparation) served as an initial criterion of resolution. Flow cytometric analysis revealed a significant increase in the number of $CD4^+Foxp3^+$ Tregs in the retina along the disease course (Fig. 5 c), representing a 2.5-fold increase in frequency. Monocyte depletion affected the number of Tregs in the retina, as indicated by a significant decrease in the frequency of $CD4^+Foxp3^+$ Tregs on d35 after immunization, compared to retinas from mice that were not treated with MC-21 (Fig. 5 d).

Finally, histopathological examination of disease severity in retinas from mice challenged for EAU and subjected to depletion of macrophages after peak disease, revealed that depletion at this phase resulted in exacerbated disease scores (Fig. 5 e, f). This result supports the notion that monocyte-derived macrophages at the later stages of EAU promote disease resolution.

Discussion

The heterogeneity of myeloid-derived cells is a well-known phenomenon in cancer (46-48), wound healing (5, 7) and was recently also described in sterile CNS trauma (10, 11). In the present study, such heterogeneity was demonstrated in an autoimmune pathological condition within the CNS, autoimmune uveitis. This diversity was manifested here by the presence of resident microglia as well as infiltrating monocyte-derived macrophages in the uveitic retina, the latter being recruited only upon disease induction. Moreover, within the infiltrating macrophage population, we identified different phenotypic subsets, the frequencies of which changed along the disease course, and which appeared to have distinct functional effects, contributing differentially to disease induction and resolution. The fact that specific depletion of the infiltrating macrophages, when performed at the resolution phase, resulted in impaired EAU resolution indicates that monocyte-derived macrophages performed a role that could not be provided by the resident cells.

Macrophage plasticity was previously demonstrated in experimental autoimmune encephalomyelitis (EAE) by an *in vitro* functional assay in which myeloid cells isolated from the CNS at different stages of the disease were capable of either activation or suppression of T cells (49). These results are consistent with our *in vivo* depletion experiments in which the absence of monocyte-derived macrophages before disease onset resulted in diminished T cell recruitment and prevented disease development, while monocyte-derived macrophage depletion at the later stage appeared to interfere with disease resolution. Another recent study in the EAE model showed that invariant natural killer T (iNKT) cell activation results in the differentiation of monocytes into an M2 phenotype and

has a positive impact on disease outcome (38). Thus, the plasticity of macrophages enables them to perform distinct and even opposing functions, which are probably influenced by the changing environmental cues within the tissue, reflecting its needs along the natural course of the disease. Whether the different macrophage subsets, as identified here, reflect the sequential recruitment of two distinct monocyte populations into the eye, or one population whose phenotype is later converted within the tissue, is an unresolved issue that has been discussed in several recent papers (5, 7, 50, 51), and is beyond the scope of the current study.

Our results suggest that the distinct effects of monocyte-derived macrophages at different stages of the disease could be mediated through expression by these cells of factors promoting immune activation/resolution and/or via their effect on Tregs. The expression of a variety of resolution markers such as mannose receptor (CD206), Dectin-1, CD204 and IL-4Rα, by the eye-infiltrating macrophages, as shown in our study, suggests their involvement in disease resolution and might account for the finding of Kerr et al., namely that myeloid cells from uveitic eyes can directly inhibit T cell proliferation *in vitro* (19). Interestingly, the infiltrating macrophages in our study were also found to express the classical anti-inflammatory mediator, IL-10, which has been shown to have a protective role in EAU (52) and is an important factor in the development and function of Tregs (53-56).

It is known that macrophages can promote immune suppression by recruiting Tregs or promoting their expansion in tumor tissues, contributing to tumor escape mechanisms (54, 57). Tregs have been associated with all stages of EAU and appear to be important in clinical uveitis. Several roles have been attributed to these cells: *(i)* They set the threshold of EAU susceptibility (43); *(ii)* they accumulate in the eye during active disease (19, 42, 45); *(iii)* they are involved in inducing and maintaining remission (Silver PB et al., manuscript in preparation); and finally *(iv)* in clinical uveitis, decreased Treg number or function has been associated with disease (33, 44). Our results, showing that monocyte-derived macrophages affect the levels of Tregs in the eye, may indicate that this is one of the mechanisms by which specific macrophage subsets may be involved in disease resolution. Additionally, as it has been shown that an inflammatory environment dampens the suppressive capacity of $Foxp3^+$ Tregs (58) and impairs the conversion of T cells into Tregs (59), it is conceivable that by controlling the inflammatory environment in the eye, the resolution-associated infiltrating macrophages characterized in our study enable the Tregs to perform their regulatory functions at the resolution phase. Regardless of whether they might act directly or through other cells, our results indicate that even in a pathology such as EAU, which is immune-induced, certain macrophage subtypes have an essential role in restoring immune homeostasis; these results are consistent with our previous studies in a model of non-inflammatory insult to the eye induced by glutamate toxicity (10).

Several autoimmune diseases in humans, including posterior uveitis, show a relapsing-remitting pattern, in which patients exhibit fluctuations in inflammatory activity as part of the natural course of the disease. In EAU, which serves as an animal model of posterior uveitis, disease typically reaches a phase of resolution, characterized by scarring and gliosis of the retina and decreased inflammatory infiltrate. However, in the C57BL/6 mouse strain, used in our study, the retina does not return to normal in terms of leukocyte levels; there are fluctuations in the numbers of both macrophages and T cells at the later phases of disease (19, 60). It has been suggested that this resolution pattern is facilitated by regulatory populations, which keep the disease in check by limiting the inflammatory infiltrate, thereby preventing disease relapse (19). Our results imply that the CX_3CR1^{high} infiltrating macrophages take part in this feedback mechanism, enabling the disease to reach a state of equilibrium, rather than to relapse. It is conceivable that the relapsing-remitting nature of autoimmune diseases in patients can be partly attributed to the insufficient recruitment/

activation of the corresponding resolving macrophage population in humans, or its inadequate conversion into the required phenotype.

Immunosuppressive drugs are often prescribed to patients suffering from autoimmune disease. Such treatment might help relieve some symptoms of the disease at the early stage, presumably at disease onset, as is supported by our present findings. However, our results identifying a subset of macrophages with immune-resolving activity suggest the possibility that the disadvantage of immunosuppressive treatment could be interference with the recruitment of such cells at the advanced stages of the disease, where they appear to be essential for its resolution. Thus, the functional heterogeneity of macrophages in an autoimmune disease as demonstrated here, argues against the indiscriminate use of immunosuppressive drugs that might also interfere with those immune processes that resolve uncontrolled inflammation and are pivotal to healing. Our data thus argue in favor of therapeutic approaches aimed at inhibition or augmentation of specific immune populations at the right time, rather than at general immune suppression.

Acknowledgments

We thank Dr. Steffen Jung for providing us with the *Cx3cr1*$^{GFP/+}$ mice and for his valuable comments, Dr. David A. Copland for assistance with the EAU model, Phyllis B. Silver for assistance with the model and for supplying the IRBP total protein, and Dr. Arie Marcovich for assistance with identifying disease onset. We thank Eric Wawrousek for assistance with determining the rd8 status of the mice, Dr. Chi-Chao Chan and the NEI Histology Core for help with processing and evaluating the histological EAU scores, Dr. Tamara Berkutzki for histological processing, Dr. Gilad Kunis for assistance with i.v. injections, Margalit Azoulay for handling the animals, Dr. Hillary Voet for statistical consultation, and Dr. Shelley Schwarzbaum for editing the manuscript.

M.S. holds the Maurice and Ilse Katz Professorial Chair in Neuroimmunology.

References

1. Gordon S. Alternative activation of macrophages. Nat Rev Immunol. 2003; 3:23–35. [PubMed: 12511873]
2. Gordon S, Taylor PR. Monocyte and macrophage heterogeneity. Nat Rev Immunol. 2005; 5:953–964. [PubMed: 16322748]
3. Mantovani A, Sica A, Locati M. Macrophage polarization comes of age. Immunity. 2005; 23:344–346. [PubMed: 16226499]
4. Mosser DM, Edwards JP. Exploring the full spectrum of macrophage activation. Nat Rev Immunol. 2008; 8:958–969. [PubMed: 19029990]
5. Arnold L, Henry A, Poron F, Baba-Amer Y, van Rooijen N, Plonquet A, Gherardi RK, Chazaud B. Inflammatory monocytes recruited after skeletal muscle injury switch into antiinflammatory macrophages to support myogenesis. J Exp Med. 2007; 204:1057–1069. [PubMed: 17485518]
6. Geissmann F, Jung S, Littman DR. Blood monocytes consist of two principal subsets with distinct migratory properties. Immunity. 2003; 19:71–82. [PubMed: 12871640]
7. Nahrendorf M, Swirski FK, Aikawa E, Stangenberg L, Wurdinger T, Figueiredo JL, Libby P, Weissleder R, Pittet MJ. The healing myocardium sequentially mobilizes two monocyte subsets with divergent and complementary functions. J Exp Med. 2007; 204:3037–3047. [PubMed: 18025128]
8. Bystrom J, Evans I, Newson J, Stables M, Toor I, van Rooijen N, Crawford M, Colville-Nash P, Farrow S, Gilroy DW. Resolution-phase macrophages possess a unique inflammatory phenotype that is controlled by cAMP. Blood. 2008; 112:4117–4127. [PubMed: 18779392]
9. Shechter R, Miller O, Yovel G, Rosenzweig N, London A, Ruckh J, Kim KW, Klein E, Kalchenko V, Bendel P, Lira SA, Jung S, Schwartz M. Recruitment of beneficial M2 macrophages to injured spinal cord is orchestrated by remote brain choroid plexus. Immunity. 2013; 38:555–569. PubMed: 23477737. [PubMed: 23477737]

10. London A, Itskovich E, Benhar I, Kalchenko V, Mack M, Jung S, Schwartz M. Neuroprotection and progenitor cell renewal in the injured adult murine retina requires healing monocyte-derived macrophages. J Exp Med. 2011; 208:23–39. [PubMed: 21220455]
11. Shechter R, London A, Varol C, Raposo C, Cusimano M, Yovel G, Rolls A, Mack M, Pluchino S, Martino G, Jung S, Schwartz M. Infiltrating blood-derived macrophages are vital cells playing an anti-inflammatory role in recovery from spinal cord injury in mice. PLoS Med. 2009; 6:e1000113. [PubMed: 19636355]
12. Simard AR, Soulet D, Gowing G, Julien JP, Rivest S. Bone marrow-derived microglia play a critical role in restricting senile plaque formation in Alzheimer's disease. Neuron. 2006; 49:489–502. [PubMed: 16476660]
13. Kang J, Rivest S. MyD88-deficient bone marrow cells accelerate onset and reduce survival in a mouse model of amyotrophic lateral sclerosis. J Cell Biol. 2007; 179:1219–1230. [PubMed: 18086918]
14. Schwartz M, Shechter R. Systemic inflammatory cells fight off neurodegenerative disease. Nat Rev Neurol. 2010; 6:405–410. [PubMed: 20531383]
15. Forrester JV, Liversidge J, Dua HS, Towler H, McMenamin PG. Comparison of clinical and experimental uveitis. Curr Eye Res. 1990; 9(Suppl):75–84. [PubMed: 2143464]
16. Caspi, RR. The Role of Cytokines in Induction and Regulation of Autoimmune Uveitis. In: Kuchroo, VK.; Sarvetnick, N.; Hafler, DA.; Nicholson, LB., editors. Contemporary Clinical Neuroscience: Cytokines and Autoimmune Diseases. 2001.
17. Dick AD, Kreutzer B, Laliotou B, Forrester JV. Phenotypic analysis of retinal leukocyte infiltration during combined cyclosporin A and nasal antigen administration of retinal antigens: delay and inhibition of macrophage and granulocyte infiltration. Ocul Immunol Inflamm. 1997; 5:129–140. [PubMed: 9234377]
18. Forrester JV, Huitinga I, Lumsden L, Dijkstra CD. Marrow-derived activated macrophages are required during the effector phase of experimental autoimmune uveoretinitis in rats. Curr Eye Res. 1998; 17:426–437. [PubMed: 9561835]
19. Kerr EC, Raveney BJ, Copland DA, Dick AD, Nicholson LB. Analysis of retinal cellular infiltrate in experimental autoimmune uveoretinitis reveals multiple regulatory cell populations. J Autoimmun. 2008; 31:354–361. [PubMed: 18838247]
20. Robertson MJ, Erwig LP, Liversidge J, Forrester JV, Rees AJ, Dick AD. Retinal microenvironment controls resident and infiltrating macrophage function during uveoretinitis. Invest Ophthalmol Vis Sci. 2002; 43:2250–2257. [PubMed: 12091424]
21. Jung S, Aliberti J, Graemmel P, Sunshine MJ, Kreutzberg GW, Sher A, Littman DR. Analysis of fractalkine receptor CX(3)CR1 function by targeted deletion and green fluorescent protein reporter gene insertion. Mol Cell Biol. 2000; 20:4106–4114. [PubMed: 10805752]
22. Mattapallil MJ, Wawrousek EF, Chan CC, Zhao H, Roychoudhury J, Ferguson TA, Caspi RR. The Rd8 mutation of the Crb1 gene is present in vendor lines of C57BL/6N mice and embryonic stem cells, and confounds ocular induced mutant phenotypes. Invest Ophthalmol Vis Sci. 2012; 53:2921–2927. [PubMed: 22447858]
23. Rolls A, Shechter R, London A, Segev Y, Jacob-Hirsch J, Amariglio N, Rechavi G, Schwartz M. Two faces of chondroitin sulfate proteoglycan in spinal cord repair: a role in microglia/macrophage activation. PLoS Med. 2008; 5:e171. [PubMed: 18715114]
24. Pepperberg DR, Okajima TL, Wiggert B, Ripps H, Crouch RK, Chader GJ. Interphotoreceptor retinoid-binding protein (IRBP). Molecular biology and physiological role in the visual cycle of rhodopsin. Mol Neurobiol. 1993; 7:61–85. [PubMed: 8318167]
25. Avichezer D, Silver PB, Chan CC, Wiggert B, Caspi RR. Identification of a new epitope of human IRBP that induces autoimmune uveoretinitis in mice of the H-2b haplotype. Invest Ophthalmol Vis Sci. 2000; 41:127–131. [PubMed: 10634611]
26. Broderick C, Hoek RM, Forrester JV, Liversidge J, Sedgwick JD, Dick AD. Constitutive retinal CD200 expression regulates resident microglia and activation state of inflammatory cells during experimental autoimmune uveoretinitis. Am J Pathol. 2002; 161:1669–1677. [PubMed: 12414514]

27. Xu H, Koch P, Chen M, Lau A, Reid DM, Forrester JV. A clinical grading system for retinal inflammation in the chronic model of experimental autoimmune uveoretinitis using digital fundus images. Exp Eye Res. 2008; 87:319–326. [PubMed: 18634784]
28. Xu H, Manivannan A, Dawson R, Crane IJ, Mack M, Sharp P, Liversidge J. Differentiation to the CCR2+ inflammatory phenotype in vivo is a constitutive, time-limited property of blood monocytes and is independent of local inflammatory mediators. J Immunol. 2005; 175:6915–6923. [PubMed: 16272351]
29. Agarwal RK, Caspi RR. Rodent models of experimental autoimmune uveitis. Methods Mol Med. 2004; 102:395–419. [PubMed: 15286397]
30. Chan CC, Caspi RR, Ni M, Leake WC, Wiggert B, Chader GJ, Nussenblatt RB. Pathology of experimental autoimmune uveoretinitis in mice. J Autoimmun. 1990; 3:247–255. [PubMed: 2397018]
31. Mack M, Cihak J, Simonis C, Luckow B, Proudfoot AE, Plachy J, Bruhl H, Frink M, Anders HJ, Vielhauer V, Pfirstinger J, Stangassinger M, Schlondorff D. Expression and characterization of the chemokine receptors CCR2 and CCR5 in mice. J Immunol. 2001; 166:4697–4704. [PubMed: 11254730]
32. Shechter R, Ziv Y, Schwartz M. New GABAergic interneurons supported by myelin-specific T cells are formed in intact adult spinal cord. Stem Cells. 2007; 25:2277–2282. [PubMed: 17540856]
33. Luger D, Silver PB, Tang J, Cua D, Chen Z, Iwakura Y, Bowman EP, Sgambellone NM, Chan CC, Caspi RR. Either a Th17 or a Th1 effector response can drive autoimmunity: conditions of disease induction affect dominant effector category. J Exp Med. 2008; 205:799–810. [PubMed: 18391061]
34. Dagkalis A, Wallace C, Hing B, Liversidge J, Crane IJ. CX3CR1-deficiency is associated with increased severity of disease in experimental autoimmune uveitis. Immunology. 2009; 128:25–33. [PubMed: 19689733]
35. Fairweather D, Cihakova D. Alternatively activated macrophages in infection and autoimmunity. J Autoimmun. 2009; 33:222–230. [PubMed: 19819674]
36. Sindrilaru A, Peters T, Wieschalka S, Baican C, Baican A, Peter H, Hainzl A, Schatz S, Qi Y, Schlecht A, Weiss JM, Wlaschek M, Sunderkotter C, Scharffetter-Kochanek K. An unrestrained proinflammatory M1 macrophage population induced by iron impairs wound healing in humans and mice. J Clin Invest. 2011; 121:985–997. [PubMed: 21317534]
37. Kerr EC, Copland DA, Dick AD, Nicholson LB. The dynamics of leukocyte infiltration in experimental autoimmune uveoretinitis. Prog Retin Eye Res. 2008; 27:527–535. [PubMed: 18723108]
38. Denney L, Kok WL, Cole SL, Sanderson S, McMichael AJ, Ho LP. Activation of Invariant NKT Cells in Early Phase of Experimental Autoimmune Encephalomyelitis Results in Differentiation of Ly6Chi Inflammatory Monocyte to M2 Macrophages and Improved Outcome. J Immunol. 2012
39. Ajami B, Bennett JL, Krieger C, McNagny KM, Rossi FM. Infiltrating monocytes trigger EAE progression, but do not contribute to the resident microglia pool. Nat Neurosci. 2011; 14:1142–1149. [PubMed: 21804537]
40. Ginhoux F, Greter M, Leboeuf M, Nandi S, See P, Gokhan S, Mehler MF, Conway SJ, Ng LG, Stanley ER, Samokhvalov IM, Merad M. Fate mapping analysis reveals that adult microglia derive from primitive macrophages. Science. 2010; 330:841–845. [PubMed: 20966214]
41. Gomez Perdiguero E, Schulz C, Geissmann F. Development and homeostasis of “resident” myeloid cells: The case of the microglia. Glia. 2013; 61:112–120. [PubMed: 22847963]
42. Caspi RR, Horai R, Chen J, Hansen A, McManigle W, Villasmil R, Silver P. Retina-specific T regulatory cells accumulate in the eye during autoimmune uveitis and act to control inflammation. J Immunol. 2011:186.
43. Grajewski RS, Silver PB, Agarwal RK, Su SB, Chan CC, Liou GI, Caspi RR. Endogenous IRBP can be dispensable for generation of natural CD4+CD25+ regulatory T cells that protect from IRBP-induced retinal autoimmunity. J Exp Med. 2006; 203:851–856. [PubMed: 16585264]
44. Sugita S, Yamada Y, Kaneko S, Horie S, Mochizuki M. Induction of regulatory T cells by infliximab in Behcet’s disease. Invest Ophthalmol Vis Sci. 2011; 52:476–484. [PubMed: 20861484]

45. Sun M, Yang P, Du L, Zhou H, Ren X, Kijlstra A. Contribution of CD4+CD25+ T cells to the regression phase of experimental autoimmune uveoretinitis. Invest Ophthalmol Vis Sci. 2010; 51:383–389. [PubMed: 19696173]
46. Gabrilovich DI, Nagaraj S. Myeloid-derived suppressor cells as regulators of the immune system. Nat Rev Immunol. 2009; 9:162–174. [PubMed: 19197294]
47. Sica A, Schioppa T, Mantovani A, Allavena P. Tumour-associated macrophages are a distinct M2 polarised population promoting tumour progression: potential targets of anti-cancer therapy. Eur J Cancer. 2006; 42:717–727. [PubMed: 16520032]
48. Umemura N, Saio M, Suwa T, Kitoh Y, Bai J, Nonaka K, Ouyang GF, Okada M, Balazs M, Adany R, Shibata T, Takami T. Tumor-infiltrating myeloid-derived suppressor cells are pleiotropic-inflamed monocytes/macrophages that bear M1- and M2-type characteristics. J Leukoc Biol. 2008; 83:1136–1144. [PubMed: 18285406]
49. Zhu B, Kennedy JK, Wang Y, Sandoval-Garcia C, Cao L, Xiao S, Wu C, Elyaman W, Khoury SJ. Plasticity of Ly-6C(hi) myeloid cells in T cell regulation. J Immunol. 2011; 187:2418–2432. [PubMed: 21824867]
50. Porta C, Rimoldi M, Raes G, Brys L, Ghezzi P, Di Liberto D, Dieli F, Ghisletti S, Natoli G, De Baetselier P, Mantovani A, Sica A. Tolerance and M2 (alternative) macrophage polarization are related processes orchestrated by p50 nuclear factor kappaB. Proc Natl Acad Sci U S A. 2009; 106:14978–14983. [PubMed: 19706447]
51. Sica A, Mantovani A. Macrophage plasticity and polarization: in vivo veritas. J Clin Invest. 2012; 122:787–795. [PubMed: 22378047]
52. Rizzo LV, Xu H, Chan CC, Wiggert B, Caspi RR. IL-10 has a protective role in experimental autoimmune uveoretinitis. Int Immunol. 1998; 10:807–814. [PubMed: 9678762]
53. Akbari O, DeKruyff RH, Umetsu DT. Pulmonary dendritic cells producing IL-10 mediate tolerance induced by respiratory exposure to antigen. Nat Immunol. 2001; 2:725–731. [PubMed: 11477409]
54. Huang B, Pan PY, Li Q, Sato AI, Levy DE, Bromberg J, Divino CM, Chen SH. Gr-1+CD115+ immature myeloid suppressor cells mediate the development of tumor-induced T regulatory cells and T-cell anergy in tumor-bearing host. Cancer Res. 2006; 66:1123–1131. [PubMed: 16424049]
55. Seo N, Hayakawa S, Takigawa M, Tokura Y. Interleukin-10 expressed at early tumour sites induces subsequent generation of CD4(+) T-regulatory cells and systemic collapse of antitumour immunity. Immunology. 2001; 103:449–457. [PubMed: 11529935]
56. O'Garra A, Vieira PL, Vieira P, Goldfeld AE. IL-10-producing and naturally occurring CD4+ Tregs: limiting collateral damage. J Clin Invest. 2004; 114:1372–1378. [PubMed: 15545984]
57. Curiel TJ, Coukos G, Zou L, Alvarez X, Cheng P, Mottram P, Evdemon-Hogan M, Conejo-Garcia JR, Zhang L, Burow M, Zhu Y, Wei S, Kryczek I, Daniel B, Gordon A, Myers L, Lackner A, Disis ML, Knutson KL, Chen L, Zou W. Specific recruitment of regulatory T cells in ovarian carcinoma fosters immune privilege and predicts reduced survival. Nat Med. 2004; 10:942–949. [PubMed: 15322536]
58. Korn T, Reddy J, Gao W, Bettelli E, Awasthi A, Petersen TR, Backstrom BT, Sobel RA, Wucherpfennig KW, Strom TB, Oukka M, Kuchroo VK. Myelin-specific regulatory T cells accumulate in the CNS but fail to control autoimmune inflammation. Nat Med. 2007; 13:423–431. [PubMed: 17384649]
59. Zhou R, Horai R, Silver PB, Mattapallil MJ, Zarate-Blades CR, Chong WP, Chen J, Rigden RC, Villasmil R, Caspi RR. The living eye "disarms" uncommitted autoreactive T cells by converting them to Foxp3(+) regulatory cells following local antigen recognition. J Immunol. 2012; 188:1742–1750. [PubMed: 22238462]
60. Oh HM, Yu CR, Lee Y, Chan CC, Maminishkis A, Egwuagu CE. Autoreactive memory CD4+ T lymphocytes that mediate chronic uveitis reside in the bone marrow through STAT3-dependent mechanisms. J Immunol. 2011; 187:3338–3346. [PubMed: 21832158]

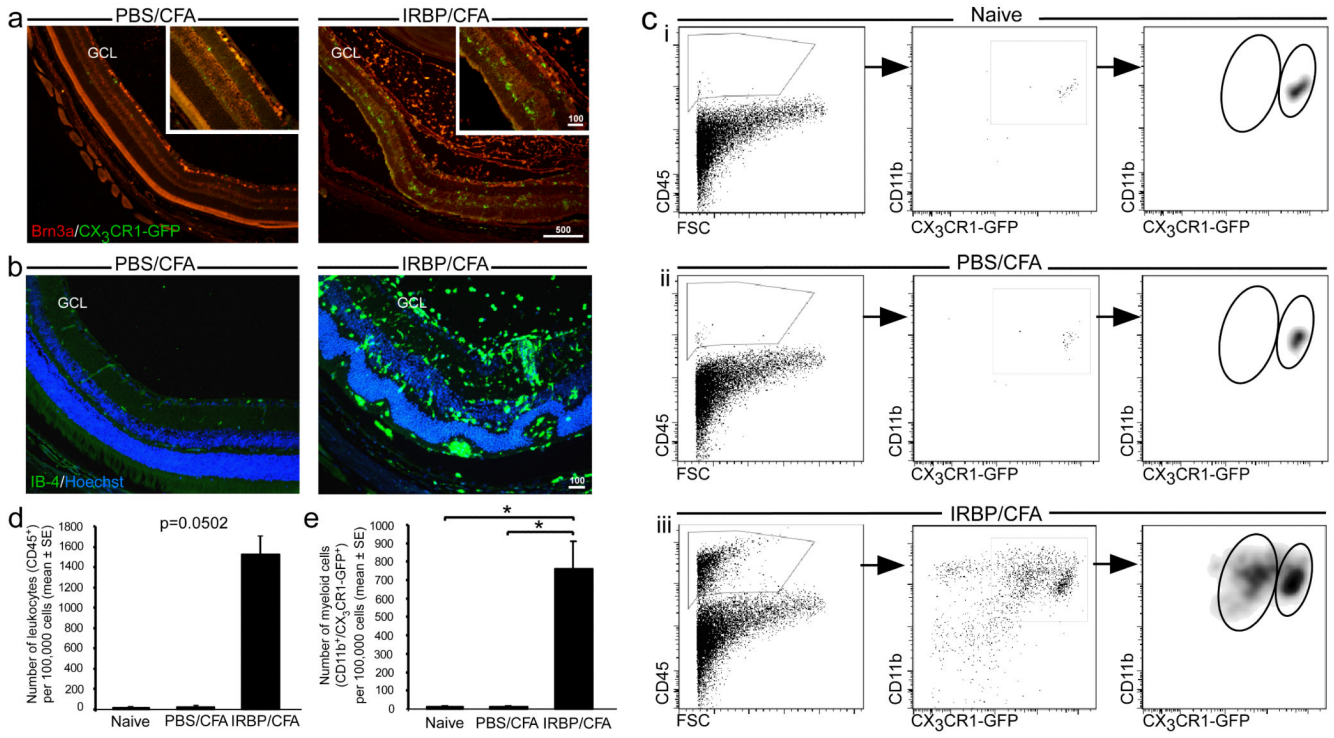

Figure 1. Changes in myeloid populations following EAU induction

Retinas taken at the peak of EAU from *Cx3cr1*$^{GFP/+}$ mice immunized with either PBS/CFA or IRBP/CFA, were analyzed by immunohistochemistry and flow cytometry (a-e). (a) Staining for Brn3a (red), a specific marker for RGCs, and for GFP (green), representing CX_3CR1^+ myeloid cells. Insets show higher magnification. Scale bars are indicated in μm. (b) Immunohistochemical analysis of IB-4$^+$ cells (green), representing activated macrophages, located in the various retinal layers, indicated by Hoechst staining (blue), including the ganglion cell layer (GCL). (c) Retinal leukocytes (CD45$^+$), analyzed for CX_3CR1-GFP and CD11b expression to identify myeloid cells, in *Cx3cr1*$^{GFP/+}$ mice either left untreated (naïve, i), or immunized with PBS/CFA (ii) or IRBP/CFA (iii). Note the appearance of the distinct CD11b$^+$CX$_3$CR1-GFP^{low} subset in the IRBP/CFA vaccinated mice, alongside an increase in CD11b$^+$CX$_3$CR1-GFP^{high} myeloid cells. Bar graphs in (d) and (e) show quantification of leukocytes and total myeloid cells, respectively, in retinas from the different groups. Graphs throughout the figure show mean ± SE of each group. *, $P < 0.05$.

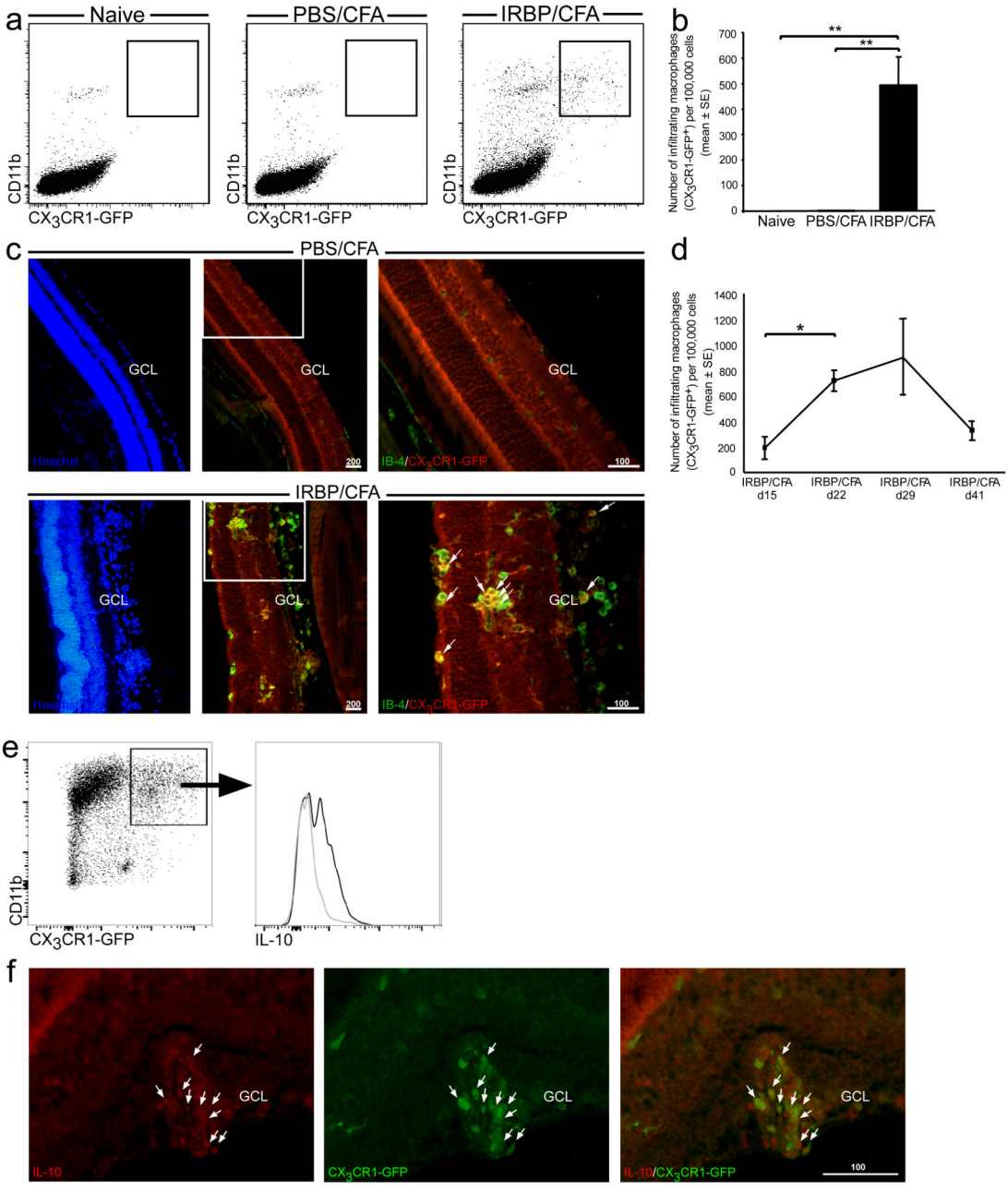

Figure 2. Monocyte-derived macrophages infiltrate diseased retinas in EAU

[$Cx_3cr1^{GFP/+}$ ➔ WT] BM chimeric mice were subjected to the EAU immunization protocol, and their retinas were analyzed for the presence of infiltrating monocyte-derived macrophages at the peak of disease (a-c). (a, b) Representative dot plots and their quantitative analysis, showing infiltration of $CD11b^+CX_3CR1\text{-}GFP^+$ monocyte-derived macrophages only to retinas from mice vaccinated with IRBP/CFA, and not to retinas from naïve or PBS/CFA-vaccinated mice. (c) Immunohistochemical analysis of retinal sections for activated infiltrating monocyte-derived macrophages. IB-4, green; CX_3CR1-GFP, red; Hoechst, blue. Scale bars are depicted in μm. Arrows indicate double-labeled cells. (d) Quantitative analysis showing the kinetics of monocyte-derived macrophage infiltration along the disease course, as analyzed by flow cytometry. (e, f) IL-10 expression by

monocyte-derived macrophages in EAU, as analyzed by flow cytometry (IL-10^{+}, black curve; isotype control, gray curve), and by immunohistochemical analysis (IL-10, red; CX_3CR1-GFP, green), respectively. Scale bars are depicted in μm. Graphs throughout the figure show mean ± SE of each group. *, $P < 0.05$; **, $P < 0.01$.

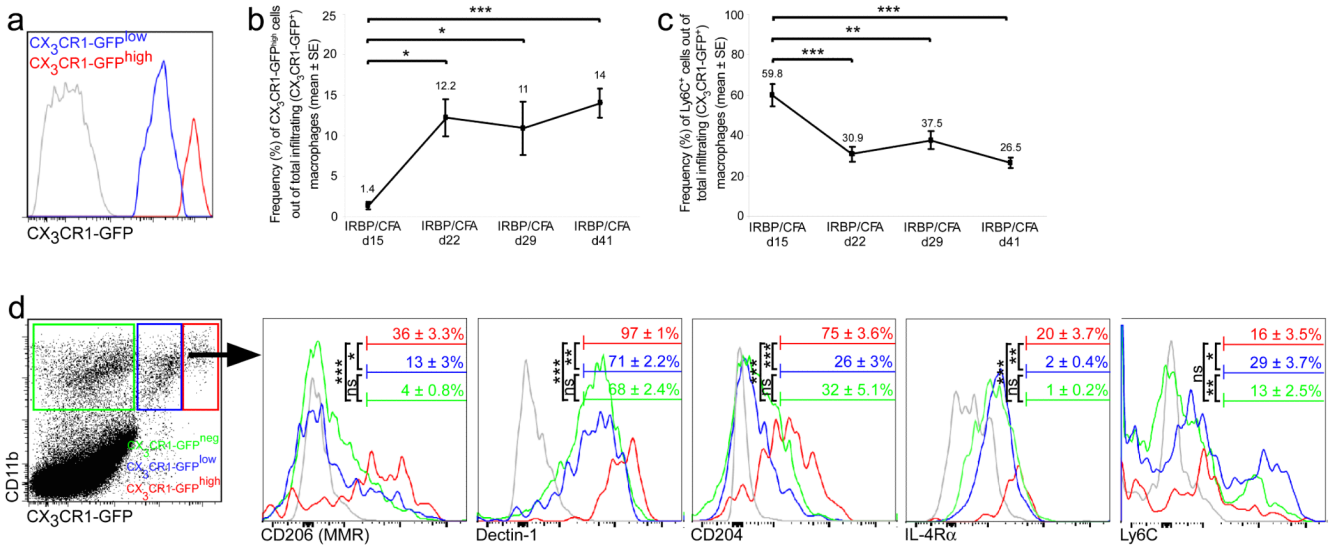

Figure 3. Monocyte-derived macrophages in EAU are a heterogeneous population

(a) $CX_3CR1\text{-}GFP^{+}$ mean fluorescence intensity of infiltrating monocyte-derived macrophages from the peak of EAU, showing that they can be divided into two subsets, $CX_3CR1\text{-}GFP^{low}$ (blue curve) and $CX_3CR1\text{-}GFP^{high}$ (red curve). (b) Quantitative analysis showing the kinetics of the frequency of $CX_3CR1\text{-}GFP^{high}$ cells out of total infiltrating macrophages along the disease course. (c) Quantitative analysis showing the kinetics of the frequency of $Ly6C^{+}$ cells out of total infiltrating macrophages along the disease course. (d) Representative histograms showing expression levels of various markers by the $CX_3CR1\text{-}GFP^{low}$ and $CX_3CR1\text{-}GFP^{high}$ infiltrating macrophages, as well as the $CX_3CR1\text{-}GFP^{neg}$ myeloid cells in the retina, at the peak of EAU. Bars demarcate cells positive for the indicated marker. Numbers above bars refer to percentage of cells positive for the indicated marker out of the relevant population; $CX_3CR1\text{-}GFP^{low}$, blue; $CX_3CR1\text{-}GFP^{high}$, red; $CX_3CR1\text{-}GFP^{neg}$, green; isotype control, gray. Graphs throughout the figure show mean ± SE of each group. *, $P < 0.05$; **, $P < 0.01$; ***, $P < 0.001$; ns, non significant.

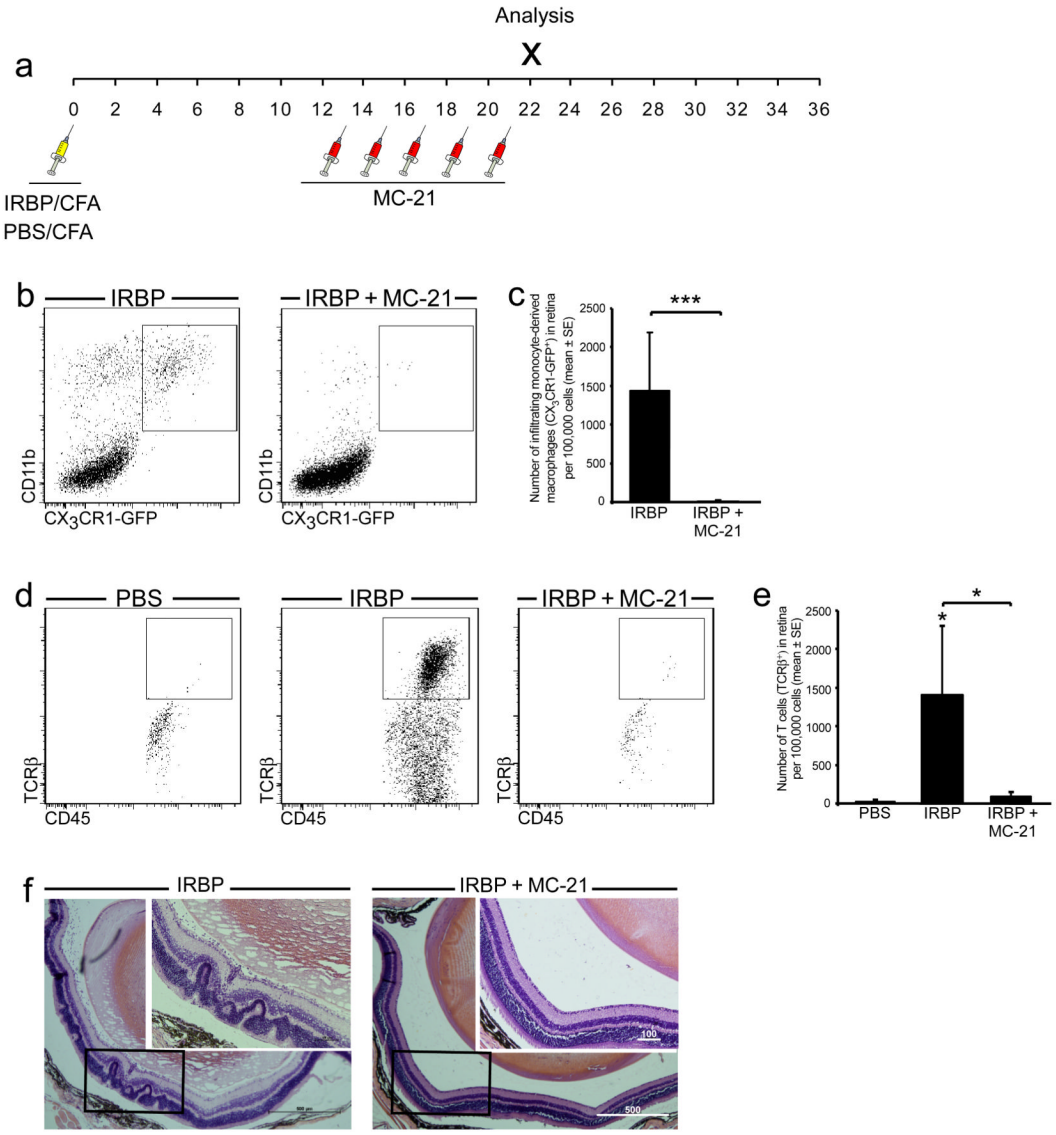

Figure 4. EAU onset is prevented in the absence of monocyte-derived macrophages

Mice were immunized with either PBS/CFA or IRBP/CFA. A group of the IRBP/CFA-immunized mice were treated with the anti-CCR2 antibody, MC-21, before the peak of EAU, as illustrated in the diagram in (a). (b, c) Representative dot plots and their quantitative analysis, showing the decrease in the infiltration of monocyte-derived macrophages to retinas of IRBP-immunized mice after MC-21 treatment. (d, e) Representative dot plots and their quantitative analysis, showing the number of T cells in IRBP-immunized mice with and without MC-21 treatment, as compared to PBS-immunized controls. Asterisks above bars indicate significant differences compared to PBS/CFA controls. Significant differences between the IRBP and IRBP + MC-21 groups are indicated by asterisks between bars. (f) Representative hematoxylin and eosin staining showing the histopathology of IRBP-immunized mice with and without MC-21 treatment. Note the typical features of EAU (massive immune infiltrate, retinal folds, vasculitis and damage to the retinal layers) in the IRBP group, all of which are absent from the MC-21-treated group. Scale bars are depicted in μm. Graphs throughout the figure show mean ± SE of each group. *, $P < 0.05$; ***, $P < 0.001$.

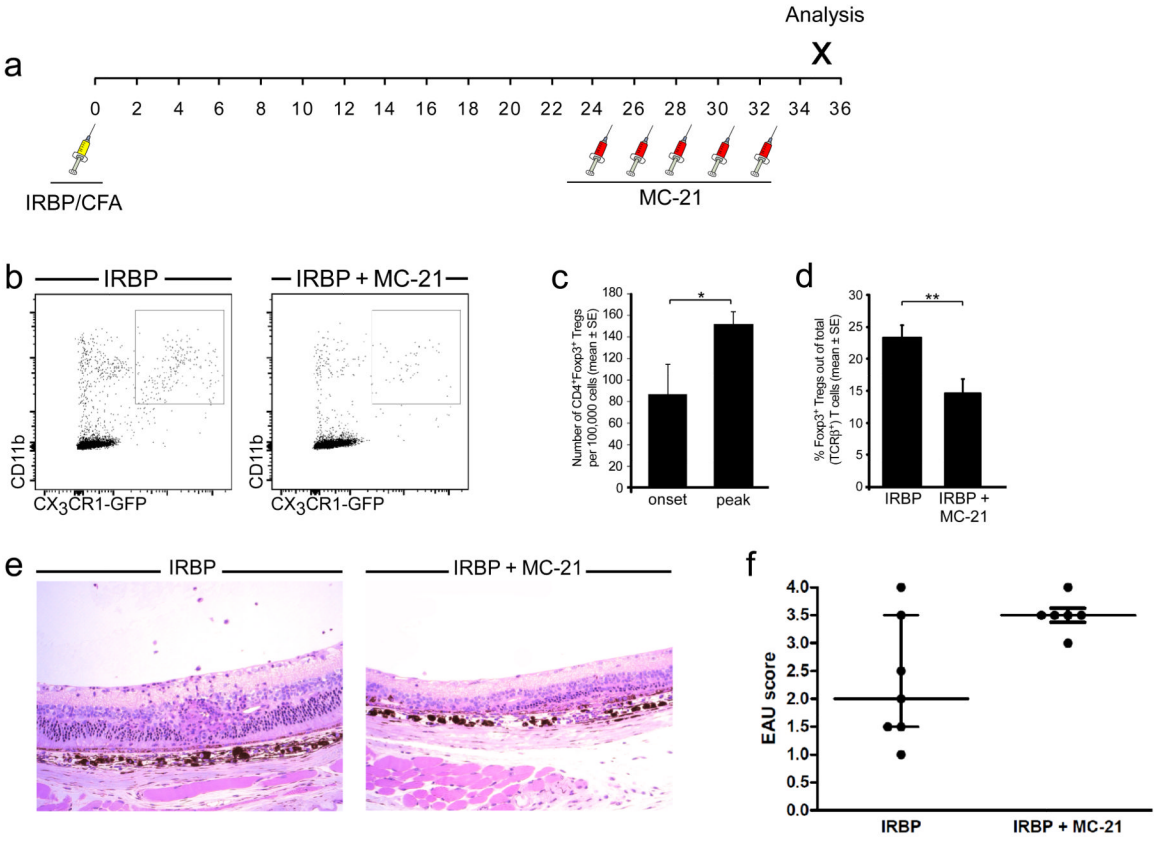

Figure 5. Monocyte-derived macrophages contribute to EAU resolution

Mice were immunized for EAU and were treated, or not, with MC-21 after the peak of disease, as illustrated in the diagram (a). (b) Representative dot plots showing the decrease in the infiltration of monocyte-derived macrophages to retinas of IRBP-immunized mice after late MC-21 treatment. (c) Quantitative analysis showing an increase in $CD4^+Foxp3^+$ Tregs after the peak of EAU. (d) Quantitative analysis showing a decrease in the frequency of $Foxp3^+$ Tregs after monocyte depletion. Graphs in (c) and (d) show mean ± SE of each group; *, $P < 0.05$; **, $P < 0.01$. (e) Representative hematoxylin and eosin staining showing the histopathology of IRBP-immunized mice with and without MC-21 treatment at the resolution phase of EAU. Note the extensive damage to the retinal layers in the MC-21-treated group. (f) EAU scores of IRBP-immunized mice with and without MC-21 treatment at the resolution phase of EAU. Graph shows median and interquartile range of each group ($p=0.077$).